Journal of the Mechanics and Physics of Solids
52 (2004) 667–689

JOURNAL OF THE MECHANICS AND PHYSICS OF SOLIDS

www.elsevier.com/locate/jmps

Plasticity size effects in free-standing submicron polycrystalline FCC films subjected to pure tension

H.D. Espinosa*, B.C. Prorok, B. Peng

Department of Mechanical Engineering, Northwestern University, 2145 Sherida Rd., Evanston, IL 60208-3111, USA

Received 3 December 2002; accepted 23 July 2003

Abstract

The membrane deflection experiment developed by Espinosa and co-workers was used to examine size effects on mechanical properties of free-standing polycrystalline FCC thin films. We present stress–strain curves obtained on films 0.2, 0.3, 0.5 and 1.0 μm thick including specimen widths of 2.5, 5.0, 10.0 and 20.0 μm for each thickness. Elastic modulus was consistently measured in the range of 53–55 GPa for Au, 125–129 GPa for Cu and 65–70 GPa for Al. Several size effects were observed including yield stress variations with membrane width and film thickness *in pure tension*. The yield stress of the membranes was found to increase as membrane width and thickness decreased. It was also observed that thickness plays a major role in deformation behavior and fracture of polycrystalline FCC metals. A strengthening size scale of one over film thickness was identified. In the case of Au free-standing films, a major transition in the material inelastic response occurs when thickness is changed from 1 to 0.5 μm. In this transition, the yield stress more than doubled when film thickness was decreased, with the 0.5 μm thick specimen exhibiting a more brittle-like failure and the 1 μm thick specimen exhibiting a strain softening behavior. Similar plasticity size effects were observed in Cu and Al. Scanning electron microscopy performed on Au films revealed that the number of grains through the thickness essentially halved, from approximately 5 to 2, as thickness decreased. It is postulated that this feature affects the number of dislocations sources, active slip systems, and dislocation motion paths leading to the observed strengthening. This statistical effect is corroborated by the stress–strain data in the sense that data scatter increases with increase in thickness, i.e., plasticity activity.

The size effects here reported are the first of their kind in the sense that the measurements were performed on free-standing polycrystalline FCC thin films subjected to macroscopic

* Corresponding author. Tel.: +1-847-467-5989; fax: +1-847-491-3915.
E-mail address: espinosa@northwestern.edu (H.D. Espinosa).

0022-5096/$ - see front matter
doi:10.1016/j.jmps.2003.07.001

homogeneous axial deformation, i.e., in the absence of deformation gradients, in contrast to nanoindentation, beam deflection, and torsion, where deformation gradients occur. To the best of our understanding, continuum plasticity models in their current form cannot capture the observed size scale effects.

Keywords: Thin films; Plasticity; Strengthening; MEMS; Failure

1. Introduction

Knowledge of a material's mechanical properties has long been essential to the design and development of structures and systems. At the millimeter or larger size scale, these properties are well known for most materials and well-established testing procedures and constitutive models are available. Specimens at this size scale typically have dimensions far exceeding the scale of the underlying material microstructure. Hence, homogenization and averaging schemes are used to interpret experiments and formulate constitutive models.

Over the past decade, there has been a substantial thrust to reduce the size of many electronic and electromechanical systems to the micron and sub-micron scale by fabricating devices out of thin film materials. In these applications, successful device development requires a thorough understanding of thin film mechanical properties. At this scale, device geometry and dimensions are similar in size to the material microstructural features. Therefore, tests capable of accurately measuring the effect of microstructure on mechanical properties need to be used (Espinosa et al., 2001a, b, 2003). In this article, we report unique findings in this regard.

1.1. Size effects

The mechanical response of thin films depends on many factors. Of main relevance is the existence of film thickness effects that arise because of geometrical constraints on dislocation motion. Size effects on mechanical properties begin to play a dominant role when one or more of the structure's dimensions begin to approach the scale of the material microstructural features. For thin films and MEMS materials this characteristic dimension is on the order of 0.1–10.0 μm. At this size scale, there is no significant effect on the material elastic properties since they depend on the bonding nature between the constituent atoms. By contrast, the onset of plastic deformation depends strongly on the ability of dislocations to move under an induced stress (Nix, 1989; Weertman and Weertman, 1992; Hull and Bacon, 1984; Arzt, 1998). The ease of their movement can be hindered by any number of obstacles such as grain boundaries, precipitates, twins, forest dislocation, and interfaces. Specimen size then begins to govern plastic behavior by creating geometrical constraints and surface effects, which force dislocations to move only in preferred directions. Other effects that specimen size can have on plastic deformation involve microstructural features. This includes grain size, morphology, and crystallographic texture. Preferential grain orientations during film growth result from minimization of surface energies (Borodkina and Orekhova, 1982; Lejeck and Sima, 1983). Likewise, the average grain size scales with the film thickness due to an effect called the "specimen thickness effect," which depends upon grain boundaries being pinned by their surface grooves, occurring when the mean equivalent grain diameter is on the order of the film thickness (Beck et al., 1948; Mullins, 1958).

Several pioneering studies have experimentally identified the existence of size effects on plasticity of *polycrystalline* metals. Fleck et al. (1994) investigated plasticity size effects by applying a torque to copper rods of varying diameter in the range of 12–170 μm. An increase in strength by a factor of three was observed for the smallest diameter wire over the largest. Ma and Clark (1995), obtained experimental nanoindentation data showing a strong size effect on material hardness. They found that hardness decreases as indentation depth increases. Their results were verified and extended in subsequent studies (Atkinson, 1995; Poole et al., 1996; Nix, 1997; Nix and Gao, 1998; McElhaney et al., 1998; Begley and Hutchinson, 1998; Goken et al., 1999; Stölken and Evans, 1998) identified plasticity size effects in the bending of strips, of varying thickness between 12 and 50 μm, around a rigid rod. The experimental results showed a strength increase for the thinner films over the thicker films. These studies motivated the investigation of the nature of size effects at this scale.

In these pioneering studies, the size dependence of the mechanical properties has been considered to be a result of non-uniform straining (Fleck and Hutchinson, 1993; Fleck et al., 1994; Nix and Gao, 1998). It was shown that classical continuum plasticity could not predict the size dependence in this regime. The generally accepted size limit for accurate description of plasticity by the classical theory is systems with dimensions larger than 100 μm. At the other end of the spectrum, molecular mechanics can accurately describe material behavior. Due to limitations on performing atomistic simulations for more than 1 million atoms, the maximum size regime computationally approachable is systems with dimensions smaller than 0.1 μm in size (Hutchinson, 2000). This leaves an intermediate region where strain gradient plasticity theory has been proposed to describe material behavior (Aifantis, 1992; Fleck and Hutchinson, 1993, 1997; Fleck et al., 1994; Gao et al., 1999a, b; Huang et al., 2000; Hutchinson, 2000; Bazant and Guo, 2001). In the aforementioned work of Fleck et al. (1994), direct tensile tests were also performed on identically sized copper wires. The authors concluded that for the most part, no size effects existed for this case. It should be noted that the smallest rod diameter investigated by this group was 12 μm. The homogeneous manner in which the uni-axial tests were conducted appears to have hindered gradients in plasticity from occurring. The question can be raised then whether size effects exist in polycrystalline metal films possessing constant grain size, in the absence of strain gradients.

Doerner et al. (1986), Nix (1989), Venkatraman et al. (1990) and Venkatraman and Bravman (1992) examined strengthening size effects in pure Al and Al alloys thin films by means of wafer curvature measurements. Thin films were grown on passivated Si substrates and biaxial strength measured as a function of film thickness and temperature. Doerner et al. (1986) deposited films with various thicknesses, which resulted in an average grain size of about 1.3 times the film thickness. Venkatraman and Bravman

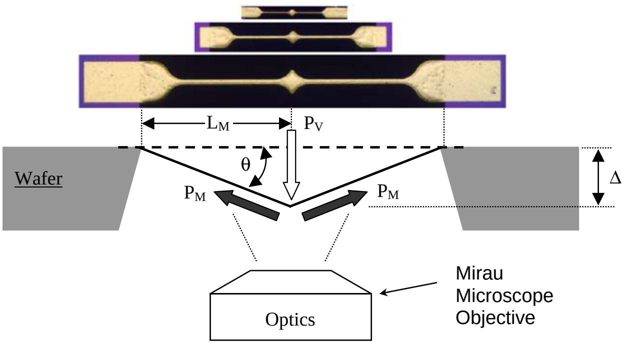

Fig. 1. Side view of the MDE test showing vertical load being applied by a nanoindenter, P_V, the membrane in-plane load, P_M, and the position of the Mirau microscope objective.

(1992) varied the film thickness by repeated growth and dissolution of an anodic oxide barrier. An approximately constant grain size of about 1μm was obtained by this approach. By separating grain size, based on the Hall-Petch relation, and thickness strengthening effects, these studies revealed a thickness strengthening effect of one over the film thickness. Nix (1989) explained this dependence by a misfit dislocation model in which work done by the applied stress must be enough to bow a dislocation and leave two dislocations at the film–substrate and film–oxide interfaces. Even when this simple model does not account for obstacles to dislocation motion such as grain boundaries, precipitates and other dislocations, it captures the main trends observed in experiments. The limitations of the model in the interpretation of size effects in polycrystalline thin films were evidenced by the measurements reported by Venkatraman and Bravman (1992). They characterized the strengthening effect as a function of temperature and observed an asymmetry between variations in strength with temperature in tension and compression. They concluded that in tension there is a strengthening mechanism, also scaling as one over the film thickness, *in addition* to the misfit dislocation mechanism. It should be noted that mechanical characterization of free-standing unpassivated thin films in the submicron regime remained elusive until recently due to the lack of a simple and robust experimental technique. Such characterization providing direct evidence of the existence of strengthening mechanisms other than the one arising from the misfit dislocation mechanism is here addressed. The membrane deflection experiment (MDE) developed by Espinosa and Prorok (2001a, b) and Espinosa et al. (2001a, b, 2003) are here employed to investigate this matter. The technique involves the stretching of a free-standing thin film membrane in a fixed–fixed configuration. The membrane is attached at both ends and spans a micromachined window beneath (see Fig. 1). A nanoindenter applies a line-load at the center of the span to achieve deflection. The geometry of the membranes is such that it contains tapered regions to eliminate boundary failure effects. The result is direct tension, in the absence of strain gradients, of a gauge region. Further details are given in Espinosa et al. (2003).

Preliminary data from MDE tests performed on thin gold membranes have indeed shown that size effects exist in the absence of strain gradients and interfaces (dislocation barriers) (Espinosa and Prorok, 2001a, b). This paper presents MDE experimental results that systematically examine thickness and width plasticity size effects on gold, copper and aluminum free-standing thin film specimens. We report on a comprehensive examination of size effects in the absence of macroscopically applied strain gradients.

2. Experimental procedure

2.1. Samples

Specially designed free-standing thin film specimens were microfabricated on (1 0 0) Si wafers. Specimen shape was defined on the wafer's topside by photolithography, e-beam evaporation and lift off. All films were grown by e-beam evaporation. Annealing was not pursued in view that the experiments are carried at room temperature. On the bottom side windows were etched through the wafer, underneath the specimens, with the purpose of creating free-standing membranes. The geometry of the suspended thin film membranes can be described best as a double dog-bone tensile specimen. A more detailed description of their fabrication, shape and specific dimensions is given in Espinosa et al. (2003). Fig. 1 shows an optical image and a schematic representation of three differently sized Au membranes. Membrane size was varied in scale to preserve the aspect ratio (length/width) of the gauge region. The geometry was chosen to minimize stress concentrations and boundary effects. Au membranes 2.5, 5, 10, and 20 μm wide were tested including membranes with thickness of 0.3, 0.5, and 1 μm for each width. Cu and Al membranes of the same width and 0.2 and 1 μm thick were also tested.

2.2. Membrane deflection experiment

The membrane deflection experiment (MDE) was used to achieve direct tensile stressing of the specimens (Espinosa et al., 2003). In this procedure, a line-load is applied with a nanoindenter to the center of the spanning membrane. Simultaneously, an interferometer focused on the bottom side of the membrane records the deflection. The result is direct tension in the gauged regions of the membrane with load and deflection measured independently. Stress–strain behavior is then determined from the independently obtained load and deflection, details of which are given in Espinosa et al. (2003).

Another important aspect of the test is the strain rate history for differently sized membranes. The following relation describes the strain rate for the MDE test as related to the rate of deflection at time t,

$$\dot{\varepsilon} = \frac{\mathrm{d}}{\mathrm{d}t}\left(\frac{\Delta L(t)}{L_{\mathrm{M}}}\right) = \frac{\Delta(t)}{L_{\mathrm{M}}\sqrt{\Delta(t)^2 + L_{\mathrm{M}}^2}}\left(\frac{\mathrm{d}\Delta}{\mathrm{d}t}\right),$$

where L_{M} is the membrane half length, $\Delta L(t)$ is the change in membrane length, and $(\mathrm{d}\Delta/\mathrm{d}t)$ is the vertical displacement rate. The $(\Delta L(t)/L_{\mathrm{M}})$ term is obtained from the geometrical relationship between L_{M} and the length of the deflected membrane at time

t (Fig. 1). From this relation, it is clear that if the vertical displacement rate is constant, the strain rate is not a constant value but increases with vertical deflection. A second observation is that for a constant vertical displacement rate, membranes with different half-length are subjected to slightly different strain rate histories. These aspects will be further discussed in the experimental results section.

3. Results and discussion

3.1. Au membrane microstructure characterization

The microstructure of the thin film gold membranes is shown in Fig. 2. It consists of grains with an average size of 250–300 nm with occasional larger grains, approximately 500 nm in size. An aspect of grains in thin films, especially for FCC and BCC metals, is that they can exhibit a preferred texture (Blicharski and Gorczyca, 1978; Nourbakhsh and Nutting, 1980, 1982; Borodkina and Orekhova, 1982; Lejeck and Sima, 1983). The standard explanation of this effect is the preferential growth of grains oriented in the lowest surface energy configuration (Grant et al., 1988; Weiland et al., 1988). In the case of gold thin films, the microstructure exhibits a $\langle 1\,1\,1 \rangle$ texture (Harris and King,

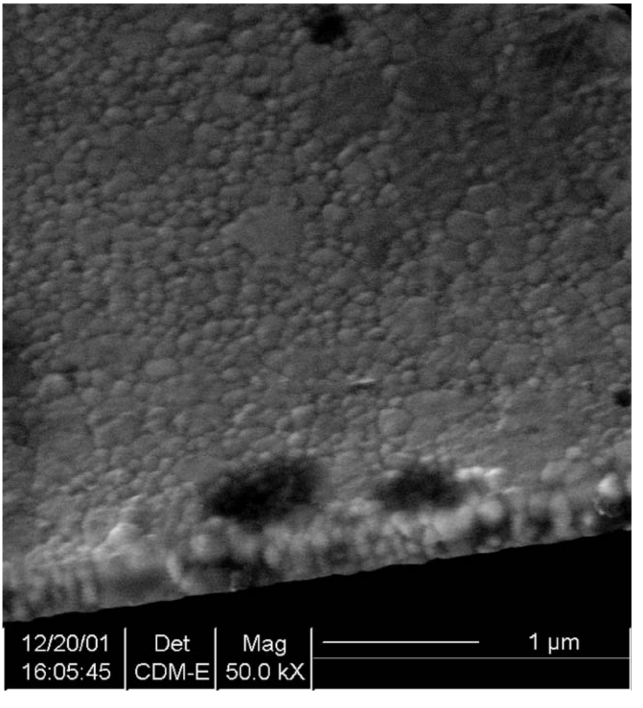

Fig. 2. SEM image showing the typical grain structure of the gold thin film specimens. Approximately 500 nm grains surrounded by smaller grains are observed at various locations along the specimen width.

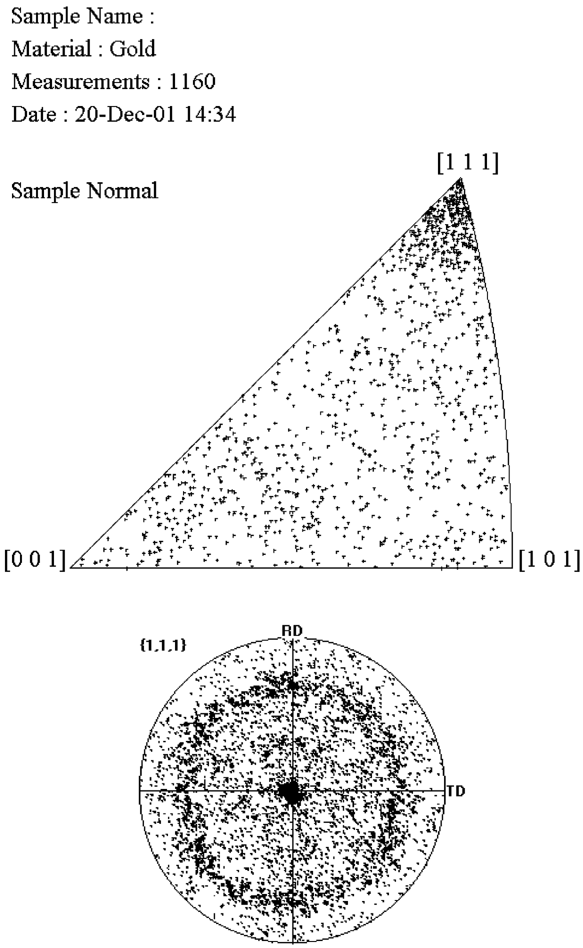

Fig. 3. Micro-diffraction results for 1 μm Au films showing a preferred ⟨1 1 1⟩ texture normal to the film surface. The experiment was also performed on 0.5 and 0.3 μm Au films. They show even a stronger texture effect.

1994, 1998). This was verified by micro-diffraction experiments (Fig. 3) showing a significant ⟨1 1 1⟩ texture in the investigated films.

Fig. 4 is SEM images showing the side view of the three studied Au membranes with different thickness. Note that a 45° tilt and different magnifications were used during imaging. Each thickness has a characteristic number of grains composing the thickness with the 0.3 μm thickness having approximately 1–2 grains, the 0.5 μm thickness having 2–3 grains, and the 1.0 μm having 3–5 grains. These observations were confirmed by transmission electron microscopy performed on film cross sections. Likewise, membranes of different widths also have a variable number of grains. Table 1 gives the average number of grains across a corresponding width. They range from

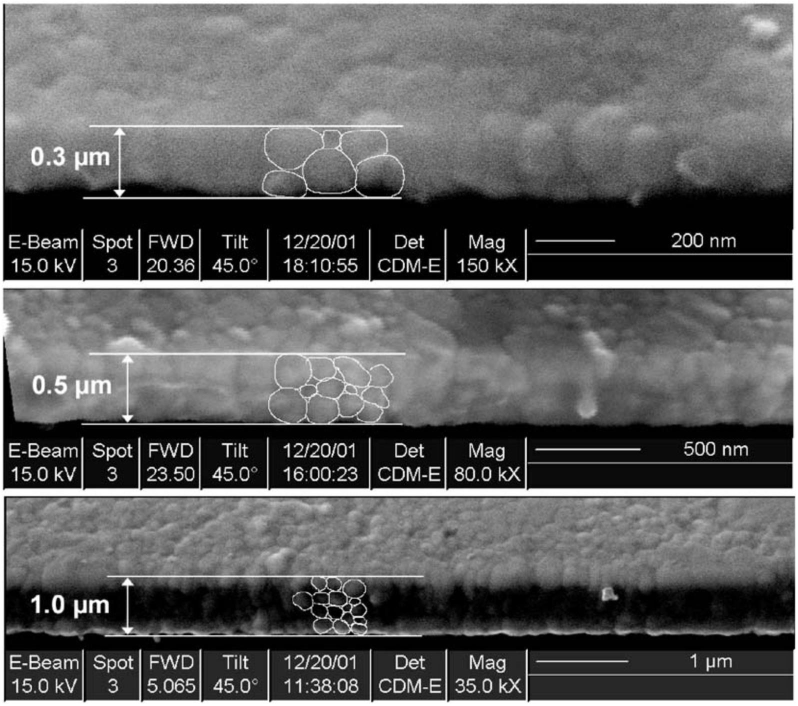

Fig. 4. SEM image highlighting the number of grains through the film thickness. Note the various magnifications and 45° tilt employed during imaging. Average grain size remains constant.

Table 1
Number of grains across membranes of different width

Width (μm)	2.5	5.0	10.0	20.0
L_M (μm)	134	209	382	362
Number of grains across the width	8–10	16–20	32–40	66–80

8 to 10 for a width of 2.5 μm to 66–80 for a width of 20 μm. These features do have an effect on the mechanical response of the membranes in the context of statistical distributions of dislocation sources, grain boundary types, and slip systems.

3.2. Effects of membrane width

Figs. 5(a)–(c) show the stress–strain curves for gold films 0.3, 0.5, and 1.0 μm thick, respectively. Each plot shows the effect of membrane width on mechanical response for widths of 2.5, 5, 10, and 20 μm. The 0.3 μm thick specimens have a well-defined elastic regime with a Young's modulus of 53–55 GPa. The specimens of widths 5, 10, and 20 μm exhibit nearly identical behavior with some variability in failure strain. The

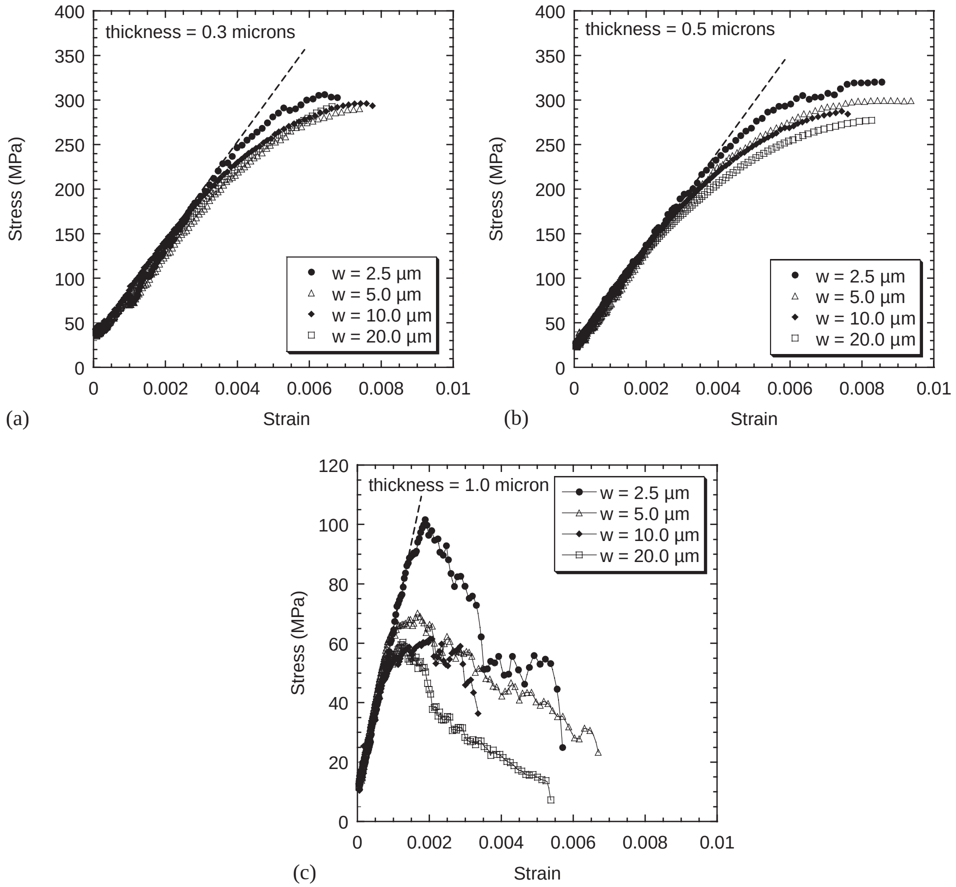

Fig. 5. Stress–strain plots comparing membrane width (2.5, 5.0, 10.0, and 20.0 μm) for a Au films 0.3 (a) 0.5 (b) and 1.0 μm (c) thick. The slope of the dashed line in each plot is between 53 and 55 GPa.

yield stress for these three widths was found to be 170 MPa. Here yield stress is defined as the stress level corresponding to departure from the linear elastic line. The 2.5 μm wide membrane shows an extended elastic zone and a larger yield stress of 220 MPa. An explanation of this behavior may arise from considering that the number of grains across the width is more or less halved each time the width is decreased. Hence an increase in geometrical constraints on deformation processes as well as statistical effects on number of dislocation sources, due to the limited number of grains across the width, can be expected. Moreover, it is known that yield stress of polycrystalline thin films can separately depend on grain size, film thickness, and crystallographic texture (Sanchez and Arzt, 1992; Thompson, 1993). Due to their small thickness and growth process, the tested gold membranes exhibit texturing with the majority of grains oriented in the $\langle 1\,1\,1 \rangle$ direction (see Fig. 3).

Table 2
Yield stresses for each combination of thickness and width with corresponding strain rate at onset of yielding

Thickness (μm)	Width (μm)	2.5	5	10	20
0.3	σ_y (MPa)	220	170	170	170
	$\dot{\varepsilon}$ (1×10^{-5} s^{-1})	5.8	3.5	1.7	0.8
0.5	σ_y (MPa)	220	170	170	140
	$\dot{\varepsilon}$ (1×10^{-5} s^{-1})	5.8	3.5	1.5	0.7
1.0	σ_y (MPa)	90	65	55	55
	$\dot{\varepsilon}$ (1×10^{-5} s^{-1})	4.5	2.2	0.9	0.3

Increasing the film thickness to 0.5 μm resulted in a similar behavior (Fig. 5(b)). As with the 0.3 μm thick membranes, all 0.5 μm thick specimens show a clearly defined elastic region with a Young's modulus of 53–55 GPa. Membrane widths of 2.5, 5, and 10 μm exhibit nearly identical behavior as in the case of 0.3 μm thick specimens. Yield stress also matched the values of the thinner specimens with 220 MPa for 2.5 μm wide membrane and 170 MPa for 5 and 10 μm wide membranes. The 20 μm wide membrane showed a marked decrease in the onset of plastic flow. Its stress–strain signature falls below the others exhibiting a lower yield stress of 140 MPa.

The 1 μm thick thin film specimens exhibited distinctly different deformation and failure behavior while preserving the feature of a decrease in yield stress with increase in specimen width. Fig. 5(c) shows the stress–strain curves for this thickness. A significant change in mechanical behavior occurs as the membranes begin to deform plastically. The failure is not a sharp and abrupt loss in load carrying capacity, but rather a gradual decrease in nominal stress with increase in deformation. The gold film ultimately fails with a sharp drop in load carrying capacity but after significant drop in the nominal stress. Also present are the appearance of sharp undulations in stress that resemble *Lüders band* effects observed in the deformation of some bulk materials, indicative of plastic yielding occurring in a discrete manner. This post-peak plastic behavior significantly differs from that observed in the thinner membranes, which exhibited strain hardening followed by sharp brittle-like rupture. It should be noted that in all cases the failure strain is below 1%.

Young's modulus for the 1 μm thick specimens was found to be 53–55 GPa, consistent with the 0.3 and 0.5 μm thick specimens. However, values of yield stress were significantly lower than in the thinner films and varied to some extent with width, although, not as significantly as in the case of thinner films. At a width of 2.5 μm the yield stress was only 90 MPa and decreased to 65 MPa for the 5 μm wide specimens and then to 55 MPa for 10 and 20 μm wide specimens.

An issue to be considered when interpreting these results is the experimentally applied strain rate. As previously mentioned, strain rate is a function of membrane half-length, which is slightly different for membranes of different width; thus, the corresponding applied strain rate is different for each membrane width. The summary of yield stress data reported in Table 2 includes the strain rate at the onset of plasticity. It is seen that yield stress changes little with strain rate, case in point being the 0.3 μm thick specimens. Therefore, the moderate difference in strain rate between specimens of different width is not considered to greatly affect the yielding behavior.

These results clearly indicate that specimen width does have a mild influence on film strength. As it will be shown later, the measured variation in yield stress with specimen width is slightly larger than the data scatter identified by repeating the test on five identically sized specimens. In the case of decreasing membrane width, it is clear that the number of grains contained in that width, especially when it falls below about 10 grains, directly affect the onset of plastic yielding. The more grains, the lower the yield stress. This could result from geometric constraints in deformation mechanisms and from strong statistical effects associated to the small number of grains, i.e., fewer dislocation sources. Membrane thickness also plays a major role in deformation behavior. In the plots presented thus far, it is a little cumbersome to directly observe thickness effects. The next section re-examines the data by plotting thickness data for membranes of equal width.

3.3. Thickness effects

Figs. 6(a), (b), (c), and (d) are the stress–strain curves for the widths of 2.5, 5, 10, and 20 μm, respectively, showing the film mechanical response as a function of thickness, i.e., 0.3, 0.5, and 1.0 μm. Vertical bars on each signature represent data scatter over five identically sized specimens. For a membrane width of 2.5 μm, the curves for membranes 0.3 and 0.5 μm thick show nearly identical elastic and plastic behavior with the exception that the 0.5 μm thick membrane exhibits a larger failure strain. Both possessed a Young's modulus of 53–55 GPa and a yield stress of 220 MPa. In both cases, plastic deformation likely occurred by the same mechanisms. As thickness was increased to 1.0 μm, deformation behavior significantly changed. Young's modulus continued to be measured at 53–55 GPa, however, yield stress decreased considerably to 90 MPa and plastic deformation occurred mostly in discrete events with an overall continual decrease in nominal stress to failure. In comparing the grain morphology through the width of the films, (Fig. 4) it can be seen that the 1 μm thick film contains 3–5 grains whereas the thinner films contain considerably less grains. We will come back to this point and its implication in the discussion section.

Stress–strain plots for a membrane width of 5 μm are shown in Fig. 6(b). As membrane width was increased, the yield stress decreased to 170 MPa for the 0.3 and 0.5 μm thick specimens and 65 MPa for the 1 μm thick. It is clear, as mentioned earlier, that the increased number of grains across the width affects deformation behavior. In the 1 μm thick membrane there appears to be a combined effect between an increase in the number of grains across the width and through the thickness to further relax statistical and geometrical constraints on deformation mechanisms.

A similar behavior is observed as membrane width is increased to 10 and 20 μm (Figs. 6(c) and (d)). The increase in both width and thickness further reduced the onset of plastic deformation as compared to the smaller specimens. Table 2 lists the yield stresses for each combination of thickness and width. A strengthening effect dominated by film thickness following a one over film thickness relationship is identified. The data

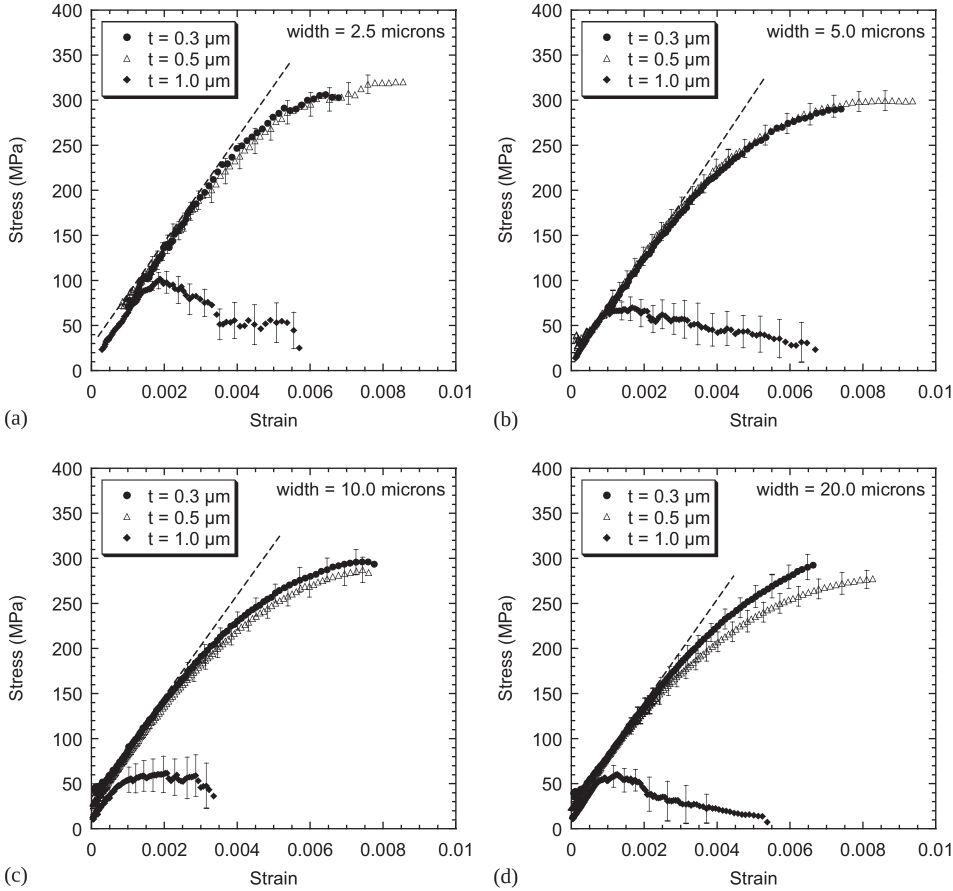

Fig. 6. Stress–strain plots comparing film thickness (0.3, 0.5, and 1.0 μm thick) for Au membrane widths of 2.5 (a), 5.0 (b), 10.0 (c), and 20.0 μm (d). The slope of the dashed line in each plot is approximately 53–55 GPa. The vertical bars on each signature represent the data scatter over five identically sized membranes. Also note the limited film ductility with values of failure strain below 1%.

indicate the existence of two behavioral regimes with thickness or width effects acting independently or in combination. The first regime is where membrane dimensions are their smallest, width = 2.5 μm and thickness = 0.3 μm. Here, the onset of plastic yielding is the highest with the grain morphology across the membrane's width consisting of 8–10 grains and 1–2 grains through the thickness (Fig. 4). It is clear that such small numbers of grains restrict the number of dislocation sources and number of dislocation motion paths available as well as the probability for intragranular deformation processes to occur. Because so few grains span the thickness and width, the sources of plastic deformation are reduced resulting in film strengthening.

The second behavioral regime exists at the upper end of the membrane dimensions, width = 20 μm and thickness = 1.0 μm. Here, the onset of plastic yielding is the lowest with the grain structure consisting of approximately 66–80 grains across the width and 4–5 grains through the thickness (Fig. 4). This assemblage of grains is beginning to approach the dimensions of a representative volume element for a polycrystalline material; hence, the reduced yield point is the result of the availability of more degrees of freedom for deformation mechanisms to occur. Of the two-dimensional changes, increasing the thickness above 0.5 μm appears to have the greatest effect in reducing yield strength, although, both appear to be acting simultaneously by their respective mechanisms. It is not clear if the lowest yield stress in this regime describes the bulk polycrystalline behavior or is merely still within the transitional regime. Thicker films need to be examined to elucidate this point.

Strain rate is not considered an issue when comparing membranes of different thickness since the specimens being compared have identical shape, i.e., same membrane half-length and width, and, therefore, identical straining history. Although the results reported in Table 2 for specimens of identical thickness indicate that the onset of plasticity occurred at slightly different strain rates, they should only be interpreted as the strain rate at which σ_y is being measured. The strain rate differences are not large enough for strain rate effects to be identified. This is a topic that is left for future investigation.

Given that all membranes of varying size and shape behave identically in the elastic region it is clear that the specimen size has a major effect only on film plasticity and strengthening. It is interesting to note that Young's modulus was consistently measured at 53–55 GPa regardless of membrane dimension and for more than 100 tested membranes. This value is significantly lower than the value of 78 GPa for bulk Au; however, values reported for thin film Au varied from 30 to 78 GPa (Nix, 1989). Since the films exhibit a strong $\langle 1\,1\,1 \rangle$ texture a low modulus may result from differences in moduli along different directions. For instance, $E_{\langle 1\,1\,1 \rangle} = 117$ GPa and $E_{\langle 1\,0\,0 \rangle} = 43$ GPa, which shows the wide degree of elastic anisotropy in Au (Courtney, 1990). Thus, with $\langle 1\,1\,1 \rangle$ primarily normal to the film surface, the measured 53–55 GPa modulus seems realistic. Given the $\langle 1\,1\,1 \rangle$ texture, one would expect that the measured Young's modulus would be consistent with calculations of the lower bound estimate (Reuss) in this plane, which yields an average modulus of 81 GPa (Corcoran, 2002). However, this estimate is significantly larger than the experimental value. The diffraction data in Fig. 3 shows a strong $\langle 1\,1\,1 \rangle$ texture, but with a fair mix of other orientations. Clearly, the lower modulus measured in the experiments is an indication of the importance of grain orientation distribution.

3.4. Results from other FCC metals

The MDE methodology was applied to test other FCC metals, namely Cu and Al. The main feature that separates these two metals from Au, is that each possesses a native oxide surface film under ambient conditions. Work by Saif et al. (2002) has shown that for submicron thick Al films this layer has no effect on the elastic properties. However, it is expected to play a role in plastic deformation by acting as a barrier to dislocations reaching the surface (Nix, 1989).

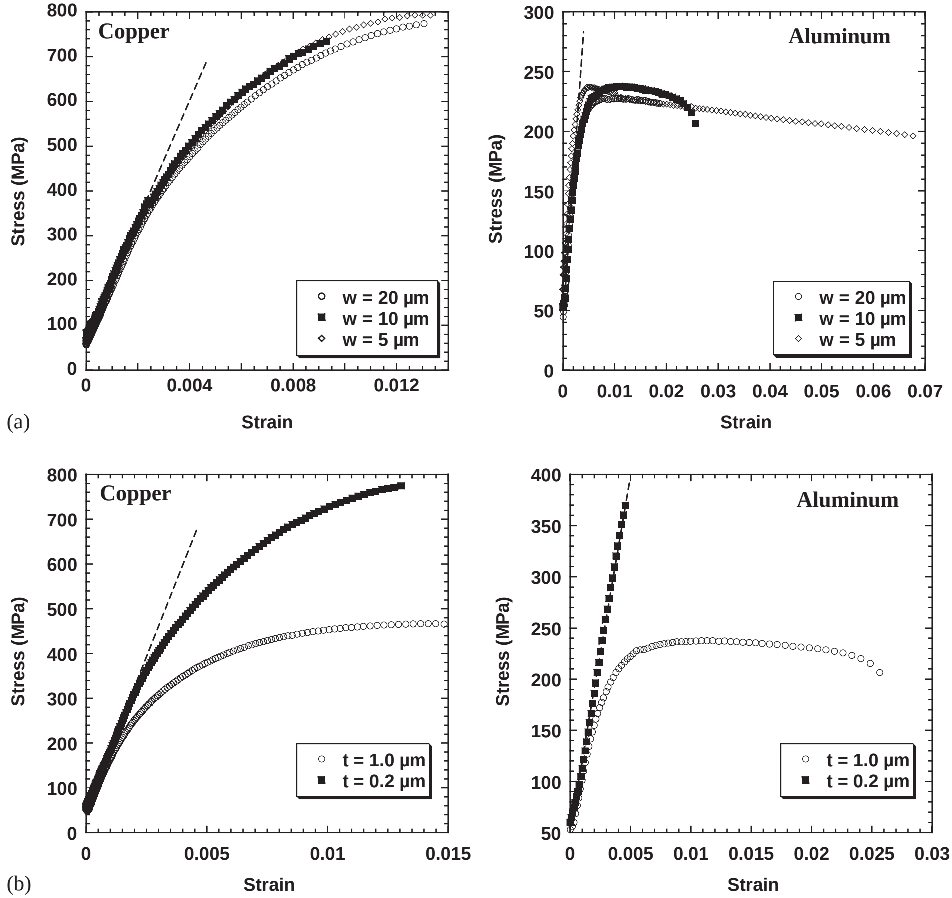

Fig. 7. Stress–strain plots for Cu and Al membranes showing effects of specimen width (a) and thickness (b).

Fig. 7(a) shows stress–strain curves for both Al and Cu that exhibit mild width effects similar to those seen in the Au membranes (Figs. 5(a)–(c)). The Cu and Al membranes have an elastic modulus of 125–129 and 65–70 GPa, respectively. For both, these values are close to that of their bulk polycrystalline forms, 121 GPa for Cu and 70 GPa for Al (Courtney, 1990). This is significantly different from the elastic behavior exhibited by the Au thin films where elastic modulus was considerably lower than the bulk polycrystalline value.

The stress–strain curves for 5, 10 and 20 μm wide specimens are compared in Fig. 7(a) for a Cu film 0.2 μm thick and an Al film 1 μm thick. The behavior for the 5 and 10 μm wide Cu membranes are nearly identical and both exhibit a yield stress of 380 MPa. As width is increased to 20 μm the yield stress decreases to approximately 345 MPa. All three specimens exhibit strain hardening until failure. A similar behavior is observed in the Al membranes having the same width but a thickness of 1 μm. Here, the yield stress is about 205 MPa for all membranes. Small variations in yield stress are observed but they fall within the data scatter. The post-yield behavior exhibited by the Al membranes is quite different (see Fig. 7(a) right).

The yield stress in Cu and Al membranes also exhibits strong thickness effects. Fig. 7(b) shows stress–strain curves for Cu and Al membranes 0.2 and 1.0 μm thick. For Cu, the yield stress more than doubles from about 160 MPa to approximately 345 MPa when thickness is decreased from 1 to 0.2 μm. Al also exhibits a similar behavior, however the 0.2 μm membranes show no evidence of plastic deformation and fail in a completely brittle manner. The yield stress of 1 μm membranes was approximately 150 MPa and the failure stress of the 0.2 μm membranes was approximately 375 MPa. Since the native oxide layer composes a larger portion of the cross-sectional area in the thinner membrane, the observed brittle behavior may be the result of brittle failure of the SiO_2 layer, which in turn may trigger inhomogeneous deformation and failure in the Al film. Prorok and Espinosa (2002) performed experiments on Au membranes *intentionally* passivated by nanometer layers of SiO_2. Their work shows that passivation may have the effect of reducing the ductility and strength of the film due to deposition induced residual stress and cracking of the passivation layer followed by localized plastic deformation of the film.

In contrast to the softening behavior observed in Au films of identical thickness, the 1 μm thick membranes of both Cu and Al showed deformation to occur in a uniform manner until failure occurs. The cause of these differences in deformation is not apparent requiring additional investigation of grain morphology, texture, dislocation structures, etc. A complete characterization of the films by X-ray and electron microscopy will be performed and reported in a future publication.

3.5. Necking and fracture observations

Fig. 8 is an SEM image of a Au membrane, 1.0 μm thick and 20 μm wide, which was stressed until failure. The image shows that the left half of the membrane slightly overlaps the right half. Several features are apparent. Multiple striations or deformation bands are seen near the failure region. They run in a direction perpendicular to the tensile load. These are regions where discrete permanent deformation has occurred on the surface of the film and may be correlated to the jogs seen in the stress–strain curves. Bands of this sort are seen in bulk materials during the development of texture with deformation (Brown, 1972). They are described as regions where grains slightly rotate to another orientation to accommodate an applied strain. Likewise, shear localization in single crystals and metallic glasses has lead to similar surface features. The formation of multiple bands is a clear indication that the membrane was uniformly loaded. The failure of the membrane can easily be described as ductile in nature. Along the fracture surface, which is perpendicular to the tensile direction but at an angle through the thickness, as observed by TEM imaging of cross sections, the gold appears to have undergone large localized plastic deformation with ductile like fingers in the stretching direction. Other observable features are nodules of gold on the films surface, which will be discussed later.

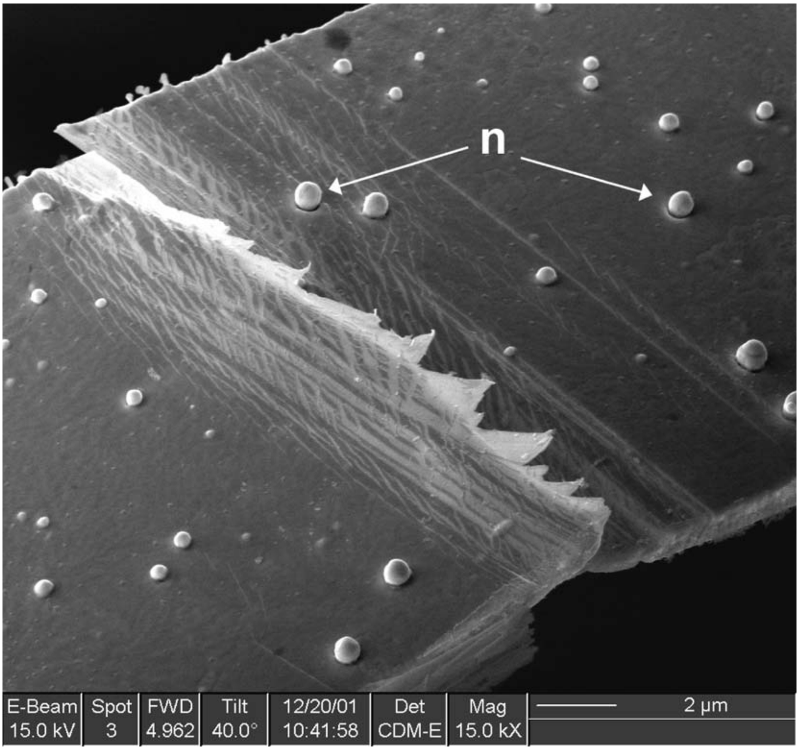

Fig. 8. SEM image of fracture for a Au film with thickness of 1.0 µm. The symbol "n" denotes nodules of gold that exist as an element of the film structure.

Some Au membranes 1 µm thick failed in the manner described above. However, in other instances, deformation and failure was observed to occur in much the same manner, but not perpendicular to the direction of tension. Fig. 9 is an SEM image of such a membrane. Here, the fracture surface is at an angle to the tensile direction. Multiple deformation bands are seen, some perpendicular to the tensile direction, denoted by "a", and others parallel to the fracture surface, denoted by "b". It is interesting to note the regions of transition between the two directions, denoted by "c". Another feature observable on this top-view of the membrane is the reduction in film width, in the neighborhood of the fracture plane, which is consistent with film necking. Failure of this sort is believed to result from maximum plastic dissipation along these directions due to the plate-like nature of the specimens. The question is then raised as to why some membranes failed perpendicular to the direction of tension. In such cases, a similar maximum plastic dissipation plane exists through the thickness. Fig. 8 shows thinning of the membrane thickness consistent with through-thickness necking. Statistical variations on dislocation sources and associated slip planes may explain the occurrence of both crack orientations.

Fig. 10 shows the fracture image for a membrane 0.5 µm thick and 20 µm wide. This image is illustrative of the change in deformation behavior observed in the

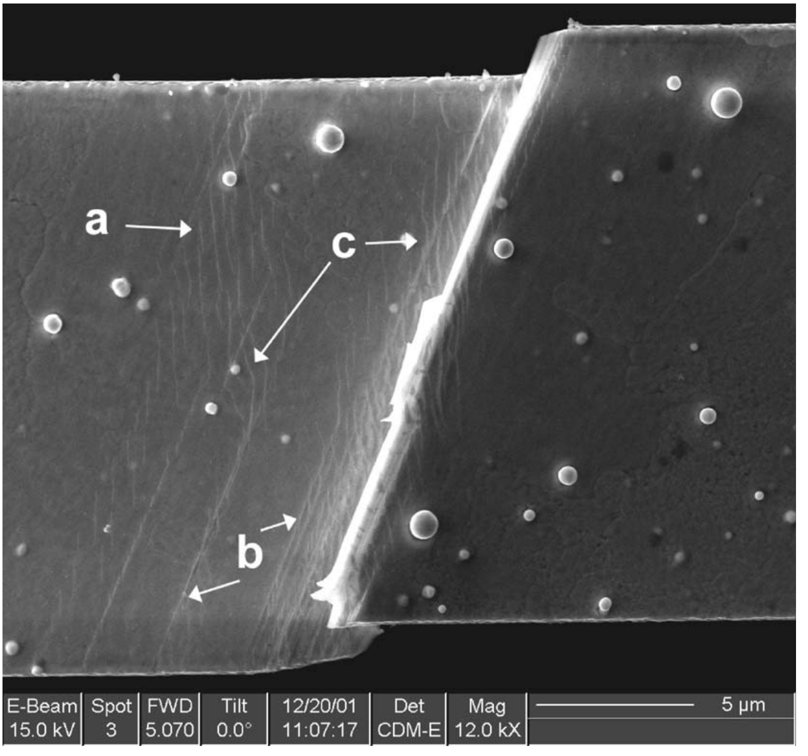

Fig. 9. SEM image of fracture for a Au film with thickness of 1.0 μm. Note that the fracture surface is not perpendicular to the tensile direction. The symbol "a" denotes deformation bands perpendicular to the tensile direction, "b" denotes those parallel to the fracture surface. And "c" denotes regions of transitions between the two.

stress–strain analysis as thickness was reduced from 1.0 to 0.5 μm. No deformation bands were observed for membranes of this thickness or thinner. Although some ductility occurred the membranes failed in a brittle-like manner. These findings are consistent with the measured stress–strain curves.

Peculiar nodules protruding from the film surfaces are seen in Figs. 8–10. These nodules are not surface contamination, but gold that exists as an actual structural feature of the films. They are positioned such that the film appears to have grown around them, e.g., the nodules denoted by "n" in Fig. 8. They are formed due to a phenomenon called "source spitting" where large droplets can be ejected from the source during e-beam deposition (Wood et al., 1981).

The post-yield behavior leading to fracture exhibited the typical statistical variations associated with plasticity and microcrack initiation. Given that all membranes of varying size and shape behaved identically in the elastic region it is clear that the specimen size had an effect on mainly the plastic deformation behavior. The uniqueness of the presented data stems from the testing technique where specimens were subjected to macroscopic homogeneous axial deformation, i.e., in the absence of

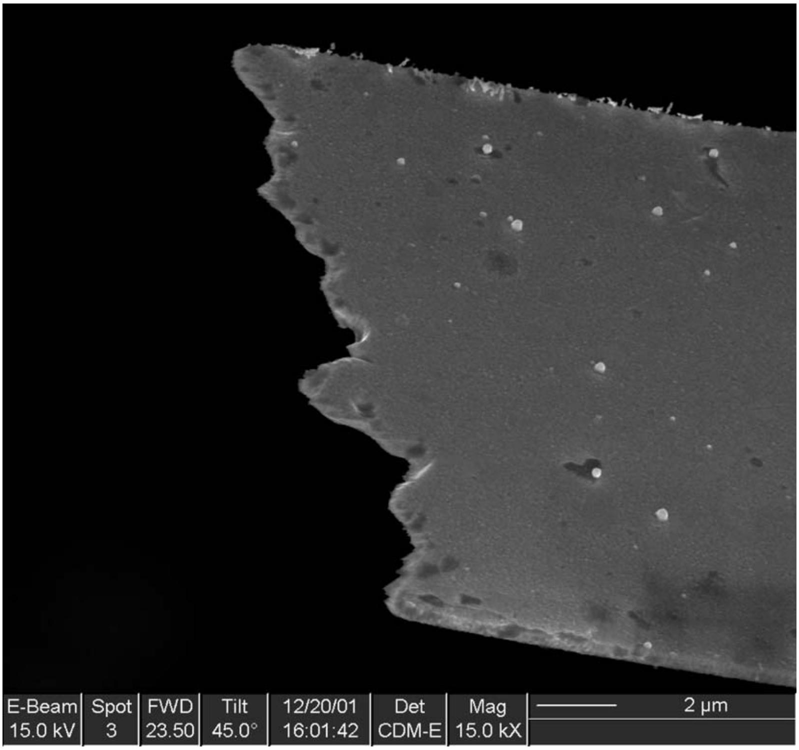

Fig. 10. SEM image of fracture for a Au film with thickness of 0.5 μm. Note the absence of deformation bands and zig-zag fracture surface.

deformation gradients, as it is the case in nanoindentation, beam deflection, and torsion tests.

3.6. Real-time observation of shear localization and fracture

Shear localization was observed in real time on some of the 1.0 μm thick membranes. Although, it appears to occur in all membranes of this thickness, based upon the stress–strain signatures, it was only observed in situ whenever the optical interferometer was imaging that particular side of the membrane. Fig. 11 shows a series of interferometric images and the corresponding stress–strain curve for a series of time intervals during MDE testing. At $t = 0$ the membrane is in the unloaded state. Note the null field obtained by proper alignment of the interferometer. At $t = 1$ the membrane had been deformed through its linear elastic region and has just begun to deform plastically. Uniform plastic deformation continues through $t = 2$. At $t = 3$ a discontinuity in the fringes appears, consistent with shear localization, and a discrete jog in the stress–strain curve is recorded. A second shear localization and corresponding jog appear at $t = 4$. The membrane finally fractures at frame $t = 5$. These images are taken from

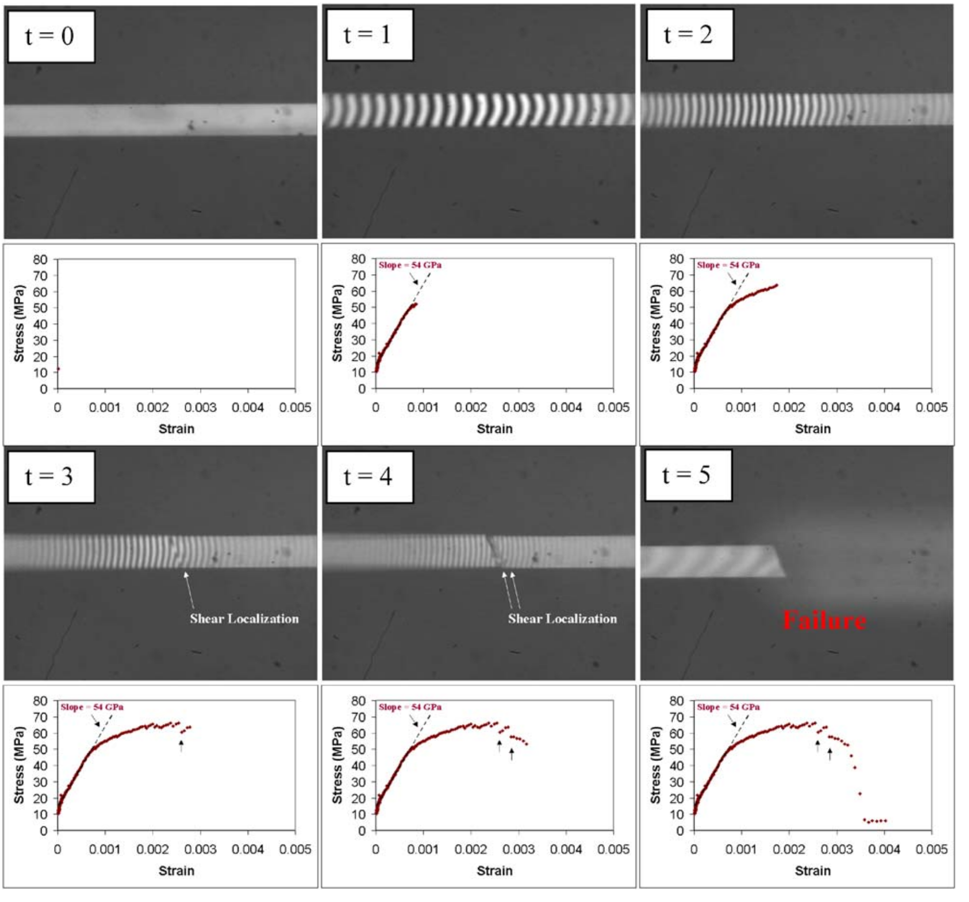

Fig. 11. Series of optical interferometric images and the corresponding stress–strain curve for different instances of time during MDE testing.

the bottom side of the membrane, which SEM image is shown in Fig. 9. In addition to the main shear localization leading to fracture, the SEM image shown in Fig. 9 shows many surface features that are believed to correspond to the smaller discrete events in the stress–strain signatures. It should be noted that in the $t = 5$ frame of Fig. 11, the stress–strain curve does not fall to zero stress after failure because half of the membrane is still engaged.

4. Conclusions

The membrane deflection experiment developed by Espinosa and co-workers was used to investigate size effects on the mechanical response of free-standing polycrystalline FCC thin films. The technique subjects free-standing films to macroscopic homogeneous axial deformation in a simple configuration. Measured stress–strain responses allow identification of film Young's modulus, onset of plastic deformation and fracture stress. Young's modulus was consistently measured at 53–55 GPa for Au specimens, 125–129 GPa for Cu specimens and 65–70 GPa for Al specimens. Measurements revealed that film width and thickness have an effect on yield stress. Although both dimensional parameters exhibited size effects, thickness, by far, had the greatest effect with a major transition in deformation behavior occurring when thickness was decreased from 1.0 to 0.5 μm. A strengthening size scale of one over the film thickness is identified. It should be noted that the misfit dislocation strengthening mechanism is not present in free-standing unpassivated Au films. Therefore, our findings constitute *direct evidence* of the existence of a strengthening mechanism other than the one arising from misfit dislocations. This finding is consistent with the work by Venkatraman and Bravman (1992), and reinforces their observations. Another important experimental result is the limited ductility exhibited by the films with strains to failure below 1% for the case of Au. This is attributed to a reduction in the degrees of freedom for plastic deformation to occur due to film texture and the small number of grains through the thickness, i.e., statistical effects associated to the existence of dislocation sources, associated slip systems, and number of dislocation motion paths. This argument is supported by the experimental data. In Fig. 6, the stress–strain data for each film thickness and width is plotted as an average of five experiments. Vertical bars represent the scatter of the data. Examination of this data reveals that scatter increases with the increase in thickness, i.e., with increase in plasticity activity within the specimen.

The implication of these findings is very important and raises a fundamental question, what yield stress should we use in the design of microelectronics and MEMS devices? Certainly, the importance of film deposition technique, substrate and thermal history has long been recognized to play a key role on film mechanical properties. Here we show that even when substrate and microfabrication processes are maintained constant, significant size effects arise in the absence of macroscopic strain gradients and passivation layers. We attribute the measured effect to material microstructural effects, e.g., texture, grain size, and in particular to the statistics of defects sources. While the size effects here reported are structure dependent, the experimental data captures the discreteness of plastic events in small volumes of material. It is postulated that dislocation mechanics in its discrete form can explain the experimental findings and predict the observed *structural* size scale relationship.

Further investigations on size effects should be pursued and a comparison of various deposition techniques and substrate effects on film growth identified. In this study, we have grown gold, copper and aluminum films by means of e-beam evaporation on a Si_3N_4 film. Other possibilities include sputtering, electrodeposition, etc. By varying the material microstructure systematically, further insight into its effects on the size dependent plasticity phenomenon could be obtained. Clearly, extensive film microstructure characterization would be needed to draw meaningful conclusions. Another key feature that needs further investigation is the effect of strain rates. Sakai et al. (1999) found that at room temperature, nanocrystalline gold with a grain size between 20 and 60 nm may exhibit creep. All of the tests reported in this work were performed at a strain rate in the regime of $1.0 \times 10^{-5}\ s^{-1}$ at room temperature.

The results reported here shed new light on deformation behavior of free-standing polycrystalline FCC thin films in the submicron regime. Analytical and computational studies are required to better understand the fundamental deformation mechanisms, particularly the mechanics of dislocation generation, motion, and interactions and the competition between inter- and intragranular deformation processes. These can be investigated through (meso) grain simulations including discrete dislocation configurations such that the role of lattice-rotation, dislocation-surface, dislocation-dislocation, dislocation-grain boundary, and dislocation-twin interactions is accounted for. Such studies will only become meaningful upon availability of a full characterization of the thin film morphology, texture and initial imperfections.

Acknowledgements

This work was sponsored by the National Science Foundation under Career Award No. CMS-9624364 and the Office of Naval Research YIP through Award No. N00014-97-1-0550. Work was also supported in part by the Nanoscale Science and Engineering Initiative of the National Science Foundation under NSF Award Number EEC-0118025. Microscopy was carried out in the Center for Microanalysis of Materials, University of Illinois, which is partially supported by the U.S. Department of Energy under grant DEFG02-96-ER45439.

References

Aifantis, E.C., 1992. On the role of gradients in the locations of deformation and fracture. Int. J. Eng. Sci. 30, 1279–1299.

Arzt, E., 1998. Size effects in materials due to microstructural and dimensional constraints: a comparative review. Acta Metall. Mater. 46, 5611–5626.

Atkinson, M., 1995. Further analysis of the size effect in indentation hardness tests of some metals. J. Mater. Res. 10, 2908–2915.

Bazant, Z., Guo, Z., 2001. Size effect asymptotic matching approximations in strain-gradient theories of microscale plasticity. Int. J. Solids Struct. 39, 5633–5657.

Beck, P.A., Kremer, J.C., Demar, L.J., Holzworth, M.L., 1948. Microstructure and grain growth of thin films. Metall. Trans. 175, 372–384.

Begley, M.R., Hutchinson, J.W., 1998. The mechanics of size-dependent indentation. J. Mech. Phys. Solids 46, 2049–2068.

Blicharski, M., Gorczyca, S., 1978. Structural inhomogeneity of deformed austenitic stainless steel. Met. Sci. 12, 303–312.

Borodkina, M.M., Orekhova, T.S., 1982. On mechanism of cubic texture formation in materials with FCC lattice. Fiz. Met. I Metalloved. 54, 1204–1207.

Brown, K., 1972. Role of deformation and shear banding in the stability of the rolling textures of aluminum and an Al–0.8% Mg alloy. J. Inst. Met. 100, 341–345.

Corcoran, S., 2002. Personal communication.

Courtney, T.H., 1990. Mechanical Behavior of Materials. McGraw-Hill, New York, p. 60.

Doerner, M.F., Gardner, D.S., Nix, W.D., 1986. Plastic properties of thin films on substrates as measured by submicron indentation hardness and substrate curvature techniques. J. Mater. Res. 1, 845–851.

Espinosa, H.D., Prorok, B.C., 2001a. Size effects of the mechanical behavior of this gold films. Proceedings of the Symposium on Mechanical Properties of MEMS Structures, the 2001 International Mechanical Engineering Congress in New York, New York, November 11–16.

Espinosa, H.D., Prorok, B.C., 2001b. Effects of film thickness on the yielding behavior of polycrystalline gold films. Mater. Res. Soc. Symp. Proc. 688, 365–372.

Espinosa, H.D., Fischer, M., Zhu, Y., Lee, S., 2001a. 3-D computational modeling of RF MEMS switches. In: Laudon, M., Romanowicz, B. (Eds.), Proceedings of the Fourth International Conference on Modeling and Simulation of Microsystems, pp. 402–406.

Espinosa, H.D., Prorok, B.C., Fischer, M., 2001b. A novel experimental technique for testing thin films and MEMS materials. Proceedings of the SEM Annual Conference on Experimental and Applied Mechanics, June 4–6, 2001, Portland, Oregon, pp. 446–469.

Espinosa, H.D., Prorok, B.C., Fischer, M., 2003. A novel method for measuring elasticity, plasticity, and fracture of thin films and MEMS materials. J. Mech. Phys. Solids 51, 47–67.

Fleck, N.A., Hutchinson, J.W., 1993. A phenomenological theory for strain gradient effects in plasticity. J. Mech. Phys. Solids 41, 1825–1857.

Fleck, N.A., Hutchinson, J.W., 1997. Strain gradient plasticity. Adv. Appl. Mech. 33, 295–361.

Fleck, N.A., Muller, G.M., Ashby, M.F., Hutchinson, J.W., 1994. Strain gradient plasticity: theory and experiment. Acta Metall. Mater. 42, 475–487.

Gao, H., Huang, Y., Nix, W.D., Hutchinson, J.W., 1999a. Mechanism-based strain gradient plasticity—I. Theory. J. Mech. Phys. Solids 47, 1239–1263.

Gao, H., Huang, Y., Nix, W.D., 1999b. Modeling plasticity at the micrometer scale. Naturwissenschaften 86, 507–515.

Goken, M., Kempf, M., Bordenet, M., Vehoof, H., 1999. Microstructural properties of superalloys investigated by nanoindentations in an atomic force microscope. Acta Mater. 47, 1043–1052.

Grant, E.M., Hansen, N., Jensen, D.J., Ralph, B., Stobbs, W.M., 1988. Texture development during grain growth in thin films. In: Kallend, J.S., Gottstein, G. (Eds.), Proceedings of the Eighth International Conference on Texture of Materials. Springer-Verlag, New York, pp. 711–716.

Harris, K.E., King, A.H., 1994. Localized texture formation and its detection in polycrystalline thin films of gold. Mater. Res. Soc. Symp. Proc. 317, 425–430.

Harris, K.E., King, A.H., 1998. Direct observation of diffusional creep via TEM in polycrystalline thin films of gold. Acta Mater. 46, 6195–6203.

Huang, Y., Gao, H., Nix, W.D., Hutchinson, J.W., 2000. Mechanism-based strain gradient plasticity—II. Analysis. J. Mech. Phys. Solids 48, 99–128.

Hull, D., Bacon, D.J., 1984. Introduction to Dislocations, 3rd Edition. Pergamon, Oxford.

Hutchinson, J.W., 2000. Plasticity at the micron scale. Int. J. Solids Struct. 37, 225–238.

Lejeck, P., Sima, V., 1983. Orientational relationships in the secondary recrystallization of pure nickel. Mater. Sci. Eng. 60, 121–124.

Ma, Q., Clark, D.R., 1995. Size dependent hardness of silver single crystals. J. Mater. Res. 10, 853–863.

McElhaney, K.W., Vlassak, J.J., Nix, W.D., 1998. Determination of indenter tip geometry and indentation contact area of depth-sensing indentation experiments. J. Mater. Res. 13, 1300–1306.

Mullins, W.W., 1958. Growth kinetics and morphology of thin films. Acta Metall. Mater. 6, 414–420.

Nix, W.D., 1989. Mechanical properties of thin films. Metall. Trans. A 20, 2217–2245.

Nix, W.D., 1997. Elastic and plastic properties of thin films on substrates. Mater. Sci. Eng. A 234–236, 37–44.

Nix, W.D., Gao, H., 1998. Indentation size effects in crystalline materials: a law for strain gradient plasticity. J. Mech. Phys. Solids 46, 411–425.

Nourbakhsh, S., Nutting, J., 1980. The high strain deformation of an aluminium–4% copper alloy in the supersaturated and aged conditions. Acta Metall. 28, 357–365.

Nourbakhsh, S., Nutting, J., 1982. Structure and properties of quenched and aged Cu–2Be after deformation to large strains. Met. Sci. 16, 323–331.

Poole, W.J., Ashby, M.F., Fleck, N.A., 1996. Micro-hardness of annealed and work-hardened copper polycrystals. Scr. Metall. Mater. 34, 564–599.

Prorok, B.C., Espinosa, H.D., 2002. Effects of nanometer thick passivation layers on the mechanical response of thin gold films. J. Nanosci. Nanotechnol. 2, 1–7.

Saif, M.T.A., Zhang, S., Haque, A., Hsia, K.J., 2002. Effect of native Al_2O_3 on the elastic response of nanoscale Al films. Acta Mater. 50, 2779–2786.

Sakai, S., Tanimoto, H., Mizubayashi, H., 1999. Mechanical behavior of high-density nanocrystalline gold prepared by gas deposition method. Acta Mater. 47, 211–217.

Sanchez, J.E., Arzt, E., 1992. Effects of grain orientation on hillock formation and grain growth in aluminum films on silicon substrates. Scr. Metall. 27, 285–290.

Stölken, J.S., Evans, A.G., 1998. A microbend test method for measuring the plasticity length scale. Acta Mater. 46, 5109.

Thompson, C.V., 1993. The yield stress of polycrystalline thin films. J. Mater. Res. 8, 237–238.

Venkatraman, R., Bravman, J.C., 1992. Separation of film thickness and grain boundary strengthening effects in Al thin films on Si. J. Mater. Res. 8, 2040–2048.

Venkatraman, R., Davies, P.W., Flinn, P.A., Fraser, D.B, Bravman, J.C., Nix, W.D., 1990. J. Electron Mater. 19, 1231.

Weertman, J., Weertman, J.R., 1992. Elementary Dislocation Theory, 2nd Edition. Oxford University Press, Oxford.

Weiland, H., Dahlem-Klein, E., Fiszer, A., Bunge, H.J., 1988. Orientation distribution of grain size classes in a grain growth texture. In: Kallend, J.S., Gottstein, G. (Eds.), Proceedings of the Eighth International Conference on Texture of Materials. Springer-Verlag, New York, pp. 717–724.

Wood, C.E.C., Rathbun, L., Ohno, H., DeSimone, D., 1981. On the origin and elimination of macroscopic defects in films. J. Cryst. Growth 51, 299–303.